bioRxiv preprint doi: https://doi.org/10.1101/706838; this version posted July 18, 2019. The copyright holder for this preprint (which was not certified by peer review) is the author/funder. All rights reserved. No reuse allowed without permission.

Connectivity domain analysis: characterization of connectivity frequency profile using filter banks

Ashkan Faghiri[a,b], Armin Iraji[a], Eswar Damaraju[a], Jessica Turner[c], Vince D. Calhoun[a,b,c]

[a] The Tri-institutional Center for Translational Research in Neuroimaging and Data Science, [Georgia State University Georgia Institute of Technology, Emory], Atlanta, GA, USA
[b] School of Electrical and Computer Engineering, Georgia Institute of Technology, Atlanta, GA 30302, USA
[c] Department of Psychology, Georgia State University, GA, USA

Abstract

Studying functional network connectivity using different imaging modalities has been the focus of many studies in recent years. One category of methods assumes that the connectivity is constant throughout the whole scanning period (e.g. using Pearson correlation to estimate linear correlation between two time series each belonging to a specific region in brain) while others relax this assumption by estimating connectivity at different time scales. The most common way to estimate dynamic functional network connectivity (dFNC) uses sliding window in combination with a connectivity estimator such as Pearson correlation (SWPC). The estimated values resulting from this method are effectively subjected to a low-pass filter (due to the sliding window) which can result in loss of connectivity information for high frequencies.

Here, we propose a new approach to estimate connectivity while preserving its full frequency range using filter banks for frequency tiling in the connectivity domain directly. This is in contrast with many other methods where frequency tiling is performed in the activity domain and indirect inferences are made about the connectivity frequency profile. Using our approach, we can estimate the full connectivity spectrum and subsequently examine both static and dynamic connectivity changes in one unified approach. In addition, the filter length (i.e. window length in SWPC) has minimal effect on the results of our approach as we are able to design our filters to have any desired band-pass range regardless of the length of filter. This method is called filter banked connectivity (FBC).

After demonstrating the approach on a simulated dataset, we use the FBC approach to estimate dFNC in a resting fMRI data set including schizophrenia patients (SZ, n=151) and healthy controls (HC, n=163). To summarize the results, we used k-means to cluster the FBC values into different clusters and calculate the total amount of time each subject spends in each cluster. These values are then compared between HC and SZ across different frequency bands. Using FBC we observed two states with very low frequency profiles where SZ patients tend to stay more in one of these states while HCs tend to stay more in the other states. In addition to common states found using SWPC, we were able to find some additional states not previously identified. These states showed very weak low frequency strength and as such SWPC was not well suited to capture them. In summary, the proposed approach offers a more comprehensive way to analyze connectivity (including both static and dynamic values).

Introduction

bioRxiv preprint doi: https://doi.org/10.1101/706838; this version posted July 18, 2019. The copyright holder for this preprint (which was not certified by peer review) is the author/funder. All rights reserved. No reuse allowed without permission.

Functional network connectivity (FNC; which estimated dependence between coherent networks typically estimated with independent component analysis) have been the focus of many neuroimaging studies over the past few decades. We can group these methods into two major categories: those that assume connectivity among different networks of the brains is constant through time (static FNC; sFNC) and those that assume temporal variation in connectivity (dynamic FNC; dFNC). Both sFNC and dFNC have proven to be extremely informative about both healthy and diseased brain function and can be used to study different neuroimaging modalities, including functional magnetic resonance imaging (fMRI).

dFNC estimation approaches

While sFNC has resulted in many interesting findings (Di Martino et al., 2008; van den Heuvel and Hulshoff Pol, 2010), this view of FNC is limited to the average connectivity patterns over the entire experiment. Approaches designed based on the dFNC idea relax the assumption of static connectivity. The most common way to estimate dFNC uses a sliding window to estimate time-varying connectivity. Typically sliding window is paired with Pearson correlation (SWPC) (Allen et al., 2014; Faghiri et al., 2018; Hutchison et al., 2013b; Kucyi and Davis, 2014). Using a sliding window to estimate dFNC has the benefit of being straightforward but it has two major shortcomings. First to use a sliding window we need to choose a window size. We want to choose a window size that is large enough so that the standard error is as small as possible while it should be small enough to allow us to detect faster changes in dFNC (Hutchison et al., 2013a). The second shortcoming of the sliding window approach is its low-pass nature (Leonardi and Van De Ville, 2015; Sakoglu et al., 2010; Thompson and Fransson, 2015). Regardless of which window size is chosen, the estimated dFNC is subjected to a low-pass filter and therefore we do not capture the full frequency range of dFNC.

Another category of methods that aim to explore the frequency profile of connectivities use time-frequency analysis ideas. The most well-known methods in this category use wavelet (Mallat, 1999). While these methods have resulted in many interesting findings in fMRI (Chang and Glover, 2010; Yaesoubi et al., 2015; Yaesoubi et al., 2017), these studies have several limitations. Firstly, the interpretation of the results in these studies can be challenging. The Chang and Glover implementation of wavelet resulted in a huge amount of information without ways to succinctly summarize the results (Chang and Glover, 2010). To remedy this, Yaesoubi et al. proposed an approach using wavelets that can be used to study group differences, but their results are all in the wavelet domain (Yaesoubi et al., 2015). This presents a difficulty in connecting the reported results to other studies on dFNC as most dFNC studies work in the time domain (the time domain results are typically considered easier to interpret).

In addition, both wavelet approaches perform frequency tiling in the activity domain instead of the connectivity domain. We believe that to discuss the frequency properties of dFNC it is important to implement all time-frequency tiling steps directly in the connectivity domain, as the relationship between activity and connectivity domain is a unknown (possibly non-linear) and therefore the frequency information is distorted when transforming from activity to connectivity domain.

Apart from the two categories of approaches mentioned above, other methods have been proposed to estimate dFNC in past years. Some of these methods are hidden Markov models (Ou et al., 2013),

bioRxiv preprint doi: https://doi.org/10.1101/706838; this version posted July 18, 2019. The copyright holder for this preprint (which was not certified by peer review) is the author/funder. All rights reserved. No reuse allowed without permission.

coactivation patterns using clustering approaches (Liu and Duyn, 2013) and window-less dictionary learning approaches (Yaesoubi et al., 2018).

Schizophrenia-related findings

There have been a number of studies of functional connectivity in schizophrenia using resting fMRI. For example, Camchong et.al. reported hyperconnectivity between default mode network (DMN) and the rest of the brain (Camchong et al., 2011). In another work, (Jafri et al., 2008) used a whole brain approach to study the differences between healthy controls (HC) and individuals with schizophrenia (SZ). They reported that SZ showed increase connectivity between DMN and visual and frontal functional domains compared to HC. Damaraju et al., reported that SZ compared to HC show increased connectivity between thalamus and sensory functional domains (Damaraju et al., 2014). Damaraju et al., also reported decreased static connectivity in sensory domains when comparing SZ to HC. Decrease connectivity in SZ compared to HC has been reported in other studies too (Erdeniz et al., 2017; Skudlarski et al., 2010). A few studies have evaluated the dynamic aspect of connectivity in SZ population. Using sliding window approach, Damaraju et al., found that SZ compared to HC tend to stay less in states which shows strong overall connectivity while they tend to spend more time in states showing weak connectivity between different domains (Damaraju et al., 2014). Other studies also reported transient reductions in both functional connectivity and networks activities (Iraji et al., 2019a; Iraji et al., 2019b). Miller et al., reported less dynamism (i.e. less change in connectivity pattern) in SZ compared to HC. For a recent review on connectivity related findings (both static and dynamic findings) in SZ population please see (Mennigen et al., 2019).

Frequency tiling in connectivity domain

In this work we aim to emphasis the idea that the connectivity domain frequency profile should be differentiated from the activity domain frequency profile. As mentioned previously, some studies have implemented frequency tiling in the activity domain and used theses tiles to make inferences about the connectivity frequency profile (which we believe is inaccurate). Here we proposed a new method to estimate connectivity which aims to implement frequency tiling directly in connectivity domain. As a central part to the approach, we use filter banks for frequency tiling in the connectivity domain (unlike wavelet methods where frequency tiling is implemented in the activity domain). We do this without making an assumption about the frequency profile of connectivity (unlike SWPC where only low-pass connectivity values can be estimated). Using filter banks, we are able to estimate the entire connectivity frequency spectrum, effectively removing the need for choosing a window size (we use a window to estimate mean and standard deviation in our approach, but this window does not impact connectivity directly as is the case for SWPC where connectivity is filtered using the window). Our proposed approach enables us to examine specific frequency bands of connectivity which includes both static connectivity (connectivity at zero frequency) and dynamic connectivity (connectivity at non-zero frequencies) in one unifying approach. In addition, the final results are in the time domain (unlike wavelet approaches where the final results are in the wavelet domain) allowing us to compare our results with other studies more easily. To summarize the results, we implemented a clustering approach as the final step of the analysis. To explain the benefits of our proposed approach we designed a limited number of simulations. In

bioRxiv preprint doi: https://doi.org/10.1101/706838; this version posted July 18, 2019. The copyright holder for this preprint (which was not certified by peer review) is the author/funder. All rights reserved. No reuse allowed without permission.

addition, to showcase the utilization of the proposed approach, we implemented it on a dataset used by our group to study sFNC and dFNC previously (Damaraju et al., 2014; Yaesoubi et al., 2017).

In the method section, we first introduce the proposed approach and its formulation. Next, all the simulations designed to evaluate the methods are explained and the dataset used in the paper is introduced briefly. All the findings are brought in the result section while in the discussion section we look at these findings more in depth. In the end, we discuss limitations and end the paper with some concluding remarks.

Materials and Methods

Filter banked connectivity

Assume we have two time series $x(t)$ and $y(t)$ where t is time. Centered SWPC at each time point ($r_{x,y}(t)$) can be estimated as follows:

$$r_{x,y}(t) = \sum_{i=t-\Delta}^{t+\Delta} \frac{[x(i) - \mu_x(t)][y(i) - \mu_y(t)]}{\sigma_x(t)\sigma_y(t)} \qquad \text{Eq. 1}$$

Where $2\Delta + 1$ is window size and $\mu_x(t)$ and $\sigma_x(t)$ are windowed sample mean and windowed standard deviation respectively (for time series x) respectively. Their definitions are as follows:

$$\mu_x(t) = \frac{1}{2\Delta + 1} \sum_{i=t-\Delta}^{t+\Delta} x(i) \qquad \text{Eq. 2}$$

$$\sigma_x(t) = \sqrt{\sum_{i=t-\Delta}^{t+\Delta} (x(i) - \mu_x(t))^2} \qquad \text{Eq. 3}$$

The same formulation can be used to estimate $\mu_y(t)$ and $\sigma_y(t)$.

Now if we define two times series $h(t)$ and $w(t)$ such that:

$$h(t) = \begin{cases} 1 & -\Delta < t < \Delta \\ 0 & otherwise \end{cases} \qquad \text{Eq. 4}$$

$$w(t) = \frac{[x(t) - \mu_x(t)][y(t) - \mu_y(t)]}{\sigma_x(t)\sigma_y(t)} \qquad \text{Eq. 5}$$

The convolution between these two time series can be written as:

bioRxiv preprint doi: https://doi.org/10.1101/706838; this version posted July 18, 2019. The copyright holder for this preprint (which was not certified by peer review) is the author/funder. All rights reserved. No reuse allowed without permission.

$$\begin{aligned} g_{x,y}(t) = h(t) * w(t) &= \sum_{i=-\infty}^{+\infty} h(t-i)w(i) \\ &= \sum_{i=-\infty}^{t-\Delta} h(t-i)w(i) + \sum_{i=t-\Delta}^{t+\Delta} h(t-i)w(i) + \sum_{i=t+\Delta}^{+\infty} h(t-i)w(i) \\ &= \sum_{i=-\infty}^{t-\Delta} 0 \times w(i) + \sum_{i=t-\Delta}^{t+\Delta} 1 \times w(i) + \sum_{i=t+\Delta}^{+\infty} 0 \times w(i) = \sum_{i=t-\Delta}^{t+\Delta} w(i) \\ &= \sum_{i=t-\Delta}^{t+\Delta} \frac{[x(i)-\mu_x(i)][y(i)-\mu_y(i)]}{\sigma_x(i)\sigma_y(i)} = g_{x,y}(t) \end{aligned} \qquad \text{Eq. 6}$$

From the $g_{x,y}(t)$ equation we can see that it is quite similar to the equation for $r_{x,y}(t)$ (i.e. SWPC at time t). Therefore, we can interpret the convolution between $h(t)$ and $w(t)$ as an approximation for SWPC. Based on the system and signal theorem (Oppenheim, 1999), we know that the output of a system with an impulse response function $h(t)$ and input of $w(t)$is $h(t) * w(t)$. So $g_{x,y}(t)$ (which can be approximated to SWPC at time t) is the output of a system with impulse response $h(t)$ where the input is $w(t)$ (Figure 1.a). The defined h_t for SWPC system is a rectangular window which can be viewed as a low-pass filter. In other words, the output of the system (SWPC estimation) is a low-pass signal and we lose the high-frequency information of the connectivity.

Filter bank is an idea that is used frequently in the electrical engineering field (Boashash, 2015). The basic idea behind filter bank is to design an array of systems to filter one time series into its different frequency sub-bands (usually non-overlapping bands that cover the whole frequency spectrum). All the filters used in this paper are Infinite impulse response (IIR) filters that have better frequency features compared to finite impulse response (FIR) filters (Rabiner et al., 1974). The issue with IIR filtering is that it has nonlinear phase (compared to linear phase for FIR filters), but because of the offline nature of fMRI data analysis we can use forward-backward filtering to achieve zero phase filtering in all our analysis (Mitra and Kuo, 2006; Oppenheim, 1999).

In our proposed approach, we replace $h(t)$ of SWPC (Figure 1.a) with a filter bank (See Figure 1.b). Each filter in the designed filter bank has its own response function $h_n(t)$ where n represents filter index. This method is called Filter banked connectivity (FBC). In FBC instead of one low-passed correlation time series (i.e. $r_{x,y}(t)$ as in SWPC), we have N time series each an estimate of connectivity in the sub frequency bands defined by $h_n(t)$. In other words:

$$r_{n,x,y}(t) = h_n(t) * w(t) \qquad n = 1, \dots, N \qquad \text{eq 7}$$

bioRxiv preprint doi: https://doi.org/10.1101/706838; this version posted July 18, 2019. The copyright holder for this preprint (which was not certified by peer review) is the author/funder. All rights reserved. No reuse allowed without permission.

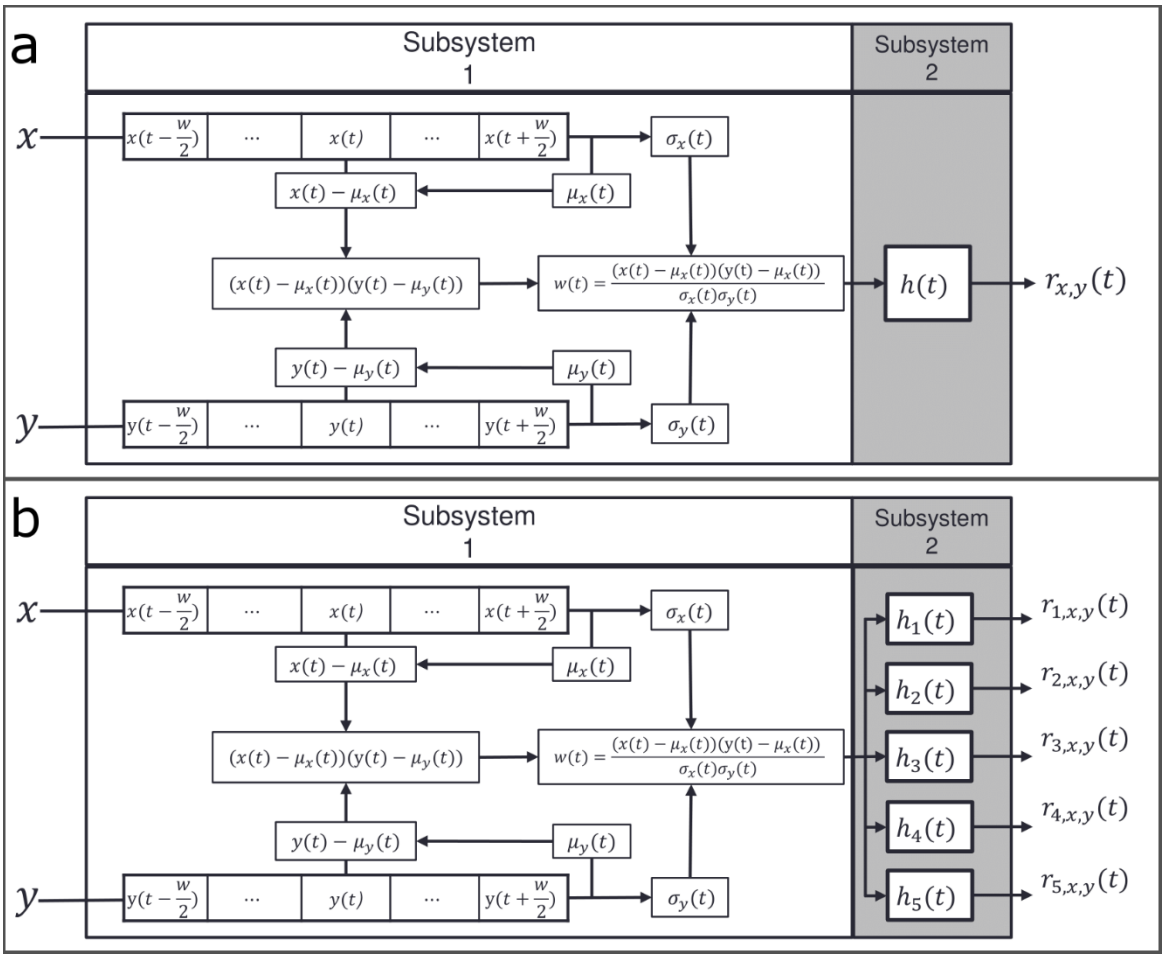

Figure 1. SWPC and FBC systems. A) SWPC system. B) FBC system. The subsystem 1 is shared between both SWPC and FBC. This subsystem uses a pair of time series and transforms activity space to connectivity space (w_t belongs to this space and has connectivity information). The difference between SWPC and FBC is in their subsystem 2 .SWPC uses a low-pass filter to calculate a low pass version of w_t while in FBC instead of a low-pass filter, an array of filters are used. These filters, include (but are not limited) to the low-pass band examined in SWPC. FBC is more flexible in the sense that it does not make any assumption about the connectivity frequency and effectively spans a range of window sizes.

Simulations

For the simulations in this paper, we use a multivariate normal distribution to simulate 6 time series:

$$X(t) \sim \mathrm{N}(\mu(t), \Sigma(t)) \qquad \text{Eq. 8}$$

For simplicity, we put μ_t equal to 0 and each time series variance equal to 1. Therefore, the covariance matrix can be written as:

$$\Sigma(t) = \begin{pmatrix} 1 & \cdots & \rho_{1,6}(t) \\ \vdots & \ddots & \vdots \\ \rho_{6,1}(t) & \cdots & 1 \end{pmatrix} \qquad \text{Eq. 9}$$

Where $\rho_{i,j}(t)$ is the correlation (i.e. connectivity) between time series i and j at time t. $\rho_{i,j}(t)$ has the form $\rho_{i,j}(t) = A_{i,j}(\mathrm{t})\cos(2\pi f_{corr} t)$. $A_{i,j}(\mathrm{t})$ forms the 6×6 matrix $A(t)$. For all simulations, we simulated time series using two connectivity states each with a length of 10,000 time points. Each state has a unique $A(t)$ and f_{corr} where f_{corr} determines the frequency of connectivity. Figure 2 shows the $A(t)$ of the two

bioRxiv preprint doi: https://doi.org/10.1101/706838; this version posted July 18, 2019. The copyright holder for this preprint (which was not certified by peer review) is the author/funder. All rights reserved. No reuse allowed without permission.

states used in all scenarios. The time series starts with state 1 and end with state 2 in all simulations, therefore, the total length of the simulated data is 20,000.

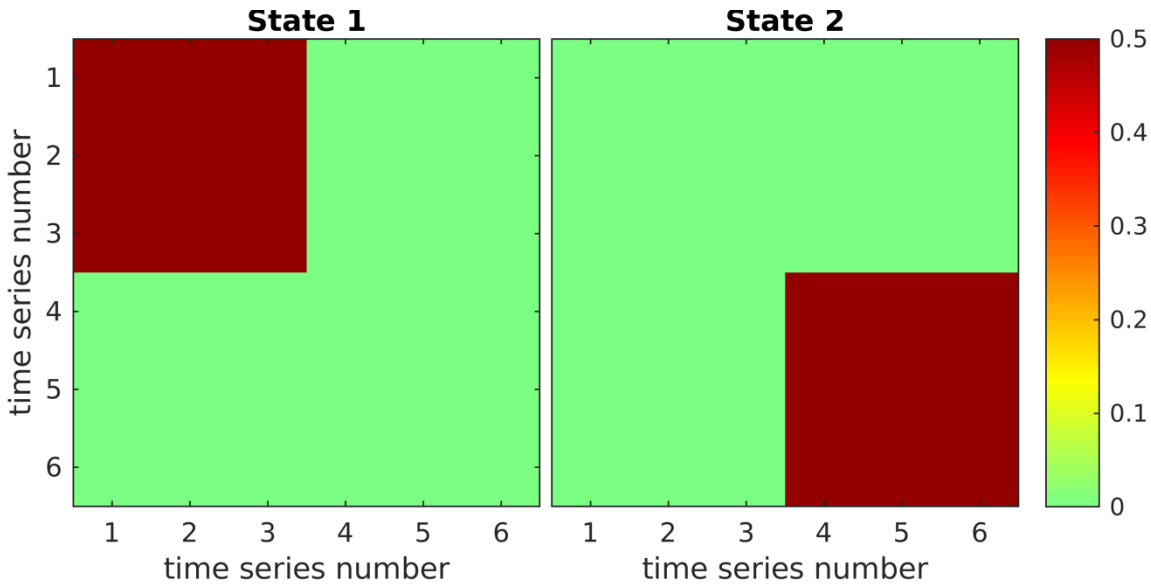

Figure 2. Correlation amplitude matrix for the two states

,Two scenarios with different values for their f_{corr} and analysis parameters were implemented. In both scenarios, we use two filter banks (one low-pass filter and one band-pass filter). In the first scenario, we chose SWPC window size such that it covers the same frequency band as the 2 designed filters. In the second scenario, the SWPC only covered the first filter bank. The first scenario represents a situation where the window size is chosen correctly (it covers all the connectivity frequencies where the information resides). On the other hand, in the second scenario, the window size is chosen larger than what should be used (i.e. it does not include some of the relevant connectivity frequencies).

To compare FBC with SWPC method, we analyzed the simulated data using both methods. To provide a more direct comparison between FBC and SWPC, the filters designed for simulation did not cover the whole spectrum of the simulation (we cannot have a window that filters the whole frequency and reach a good estimation of correlation). In addition, for simplicity purposes, we used the same window size for both FBC (window used to estimate sample mean and standard deviation) and SWPC. The f_{corr} value for each state and the designed filters frequency response will be shown when discussing the results.

The results of both FBC and SWPC were then clustered into 4 clusters using k-means approach. The reason for choosing 4 as the number of clusters was because we had 2 original states, each state has two extreme cases ($+A_t$ and $-A_t$) so we essentially have two pairs of states.

Real dataset and preprocessing

To demonstrate the utilization of FBC, we used it to analyses a resting state fMRI dataset including SZ and HC individuals. The data was obtained as a part of the Functional Imaging Biomedical Informatics Research Network (fBIRN) project (Potkin and Ford, 2009). The dataset used in this paper includes 163 HC and 151 SZ. The data acquisition and preprocessing steps are explained in our previous work (Damaraju et al.,

bioRxiv preprint doi: https://doi.org/10.1101/706838; this version posted July 18, 2019. The copyright holder for this preprint (which was not certified by peer review) is the author/funder. All rights reserved. No reuse allowed without permission.

2014). In short echo planar imaging was used to acquire 162 volumes of bold data using seven 3T MRI scanners. All scans were acquired using 2 sec as TR.

Preprocessing was started with motion correction, slice-timing correction, and despiking. Next, data were registered to a common Montreal Neurological institute (MNI) template, and a Gaussian kernel with a 6mm full width at half-maximum was used to smooth the data. For the last step of preprocessing, each voxel time series was variance normalized.

To decompose the data into 100 spatially independent time series and their associated spatial maps the pipeline proposed by Allen et al., was used (Allen et al., 2014). In the proposed approach group spatial independent component analysis (GICA) implemented in the GIFT (http://mialab.mrn.org/software/gift) software was used (Calhoun et al., 2001; Erhardt et al., 2011). First, the 162 time points for each subject were reduced into 100 dimensions using principal component analysis (PCA). All subjects' data were then concatenated and another PCA was used to reduce the dimension to 100. Finally, ICA was used to obtain 100 maximally independent components. The spatial maps of these 100 components were visually inspected and 47 components were chosen as components of interest and were grouped into 7 functional domains. The data used for the current project are exactly the same 47 components used by Damaraju et al. (Damaraju et al., 2014). The 7 functional domains are: auditory (AUD), attention/cognitive control (CC), sub-cortical (SC), Cerebellar (CB), default mode (DM), sensorimotor (SM) and visual (VIS). The spatial maps of all the components included in each functional domain can be viewed in Figure S1.

FBC and SWPC analysis (real data)

To analyze the fBIRN dataset using FBC pipeline, each component pair (pairs were selected from the pool of 47 components) was used to calculate a specific w_t (Eq. **5**) for that pair. For calculating w_t different window size values were used to explore the effect of window size on the final results. This step resulted in 1,081 w_t time series ($47 \times (47-1)/2$). All w_t were then passed through our designed filter banks. For this paper, 10 IIR filters were used to filter all the w_t values. To make sure the phase of w_t is not affected by the filters, we used a forward-backward filtering approach (Mitra and Kuo, 2006).

The filtered values resulted from all filter banks were then clustered using k-means approach. Next, we calculated how many time points each subject has spent in each state (total dwell time). This value can be calculated for all 10 frequency sub-bands separately as we have used all the sub-bands for clustering. In summary, for each state, we produce a plot that is quite similar conceptually to the frequency response of the corresponding state. In addition, we have compared the total dwell time between HC and SZ for each state.

Within this pipeline there are two analysis parameters to choose. First, we have to choose a window size which will be used to calculate w_t (i.e. calculate mean and std of component pairs). Here we have chosen a window size of 11 time points (22s) for this step. Results from other window sizes are provided in supplementary material, Figures S2 through S10. Secondly, the number of clusters (k) should be selected for k-means. We chose k = 8 as the desired number of clusters in all our analysis explained in this manuscript. Our selection was based on a metric calculated from clustering results (for more details refer

bioRxiv preprint doi: https://doi.org/10.1101/706838; this version posted July 18, 2019. The copyright holder for this preprint (which was not certified by peer review) is the author/funder. All rights reserved. No reuse allowed without permission.

to the supplementary material). In addition, we have performed our analysis using different cluster numbers and provide this information in the supplementary material (Figures S2 through S10).

Results

As mentioned in the methods section, we designed several simulation scenarios using a multivariate Gaussian pdf to demonstrate the benefits of FBC compared to SWPC. In addition, we show the utilization of FBC on real data in a comparison of SZ with HC.

Simulation Results

All the simulation results are summarized in Figure 3. Each sub figure has 7 rows. The first and fifth rows demonstrate the normalized frequency response of covariance matrix for FBC (first row) and SWPC (fifth row). The second and third rows, demonstrate the mean and standard deviation (std) of simulations' (each simulation was repeated 1000 times) centroids for FBC while the sixth and seventh rows demonstrate the same measures for SPWC results. Conceptually speaking, mean shows how the estimated values are close to the true values on average while std represent standard error of the estimators. The fourth row shows the total dwell time of each state in relation to the two filters. This information is exclusive to FBC and is absent in SWPC (SWPC is essentially one filter). Cluster 1 and 2 are the maximum and minimum values for state 1 (connectivity in state 1 oscillate between these values). Cluster 3 and 4 are the maximum and minimum values for state 2.

In the first scenario (Figure 3 a through c), the SWPC window size (10 time points) covers the same frequency band as the two filters used in FBC. This scenario includes three specific situations. In the first situation, each state f_{corr} is located in one separate filter (Figure 3a) while in the second and third situations f_{corr}s are either in the first filter (Figure 3b) or in the second filter (figure 3c). Looking at the top three rows of Figure 3, we can make several observations. The means of estimated clusters are estimated very distinctly using FBC. i.e., cluster 1 and 2 only show state 1 A_t while cluster 3 and 4 only shows state 2 A_t. In contrast, if we look at SWPC results, mean of estimated clusters are only estimated distinctly when both states have low frequencies (Figure 3b). When the frequencies of the states are higher (Figure 3a and c) mean cluster are not distinct. For example, cluster means of Figure 3c for SWPC shows both state 1 and 2 A_t in all clusters. Another interesting observation here is that for the case where the two states frequencies are located in separate filter bank frequency bands (Figure 3a), the dwell time figure for FBC clearly shows that cluster 1 and 2 happen more in first filter bank while the cluster 3 and 4 happen more in the second filter. This shows that FBC can provide correct frequency specificity in the case where connectivity frequencies are distributed in different filter frequency bands. This point will be explored more in the discussion section.

In the second scenario for the simulations, the window size is longer compared to the first scenario (30 time point) and only covers the frequency band of the first filter (Figure 3 d through f). This scenario represents the case where SWPC window size is not chosen correctly (either because of technical limitations or user choice). i.e., the frequency pass band of the SWPC window does not cover all frequencies where state connectivity frequencies are located. This is clearly shown in Figure 3d and 3f

bioRxiv preprint doi: https://doi.org/10.1101/706838; this version posted July 18, 2019. The copyright holder for this preprint (which was not certified by peer review) is the author/funder. All rights reserved. No reuse allowed without permission.

where at least one of the states has connectivity frequency outside the passband of the SWPC window. Looking at SWPC results in Figure 3d we can see that cluster 3 and 4 show very weak versions of state 2 A_t. In a more severe case where all states connectivity frequencies are outside the passband of SWPC (Figure 3f), all SWPC cluster mean values are very weak. Contrary to SWPC results, FBC mean values for cluster centroids are quite strong and similar to state 1 and 2 A_t (Figure 2).

A few other observations can be made regarding the std values. Based on the Figures 3 a through c we can see that SWPC has resulted in higher std values compared to FBC std values for null connectivity elements (matrix entries where connectivity is zero in each state). In contrast, looking at the second scenario results, we can see that using longer window sizes has resulted in lower std values when the actual connectivity frequency is very low. This is the case for Figure 3d first state and Figure 3e both states. But when the specific state has a higher frequency than the SWPC frequency band, the std values are noticeably higher for all matrices' entries. This can be seen for the second state in Figure 3d and both state results in Figure 3f.

bioRxiv preprint doi: https://doi.org/10.1101/706838; this version posted July 18, 2019. The copyright holder for this preprint (which was not certified by peer review) is the author/funder. All rights reserved. No reuse allowed without permission.

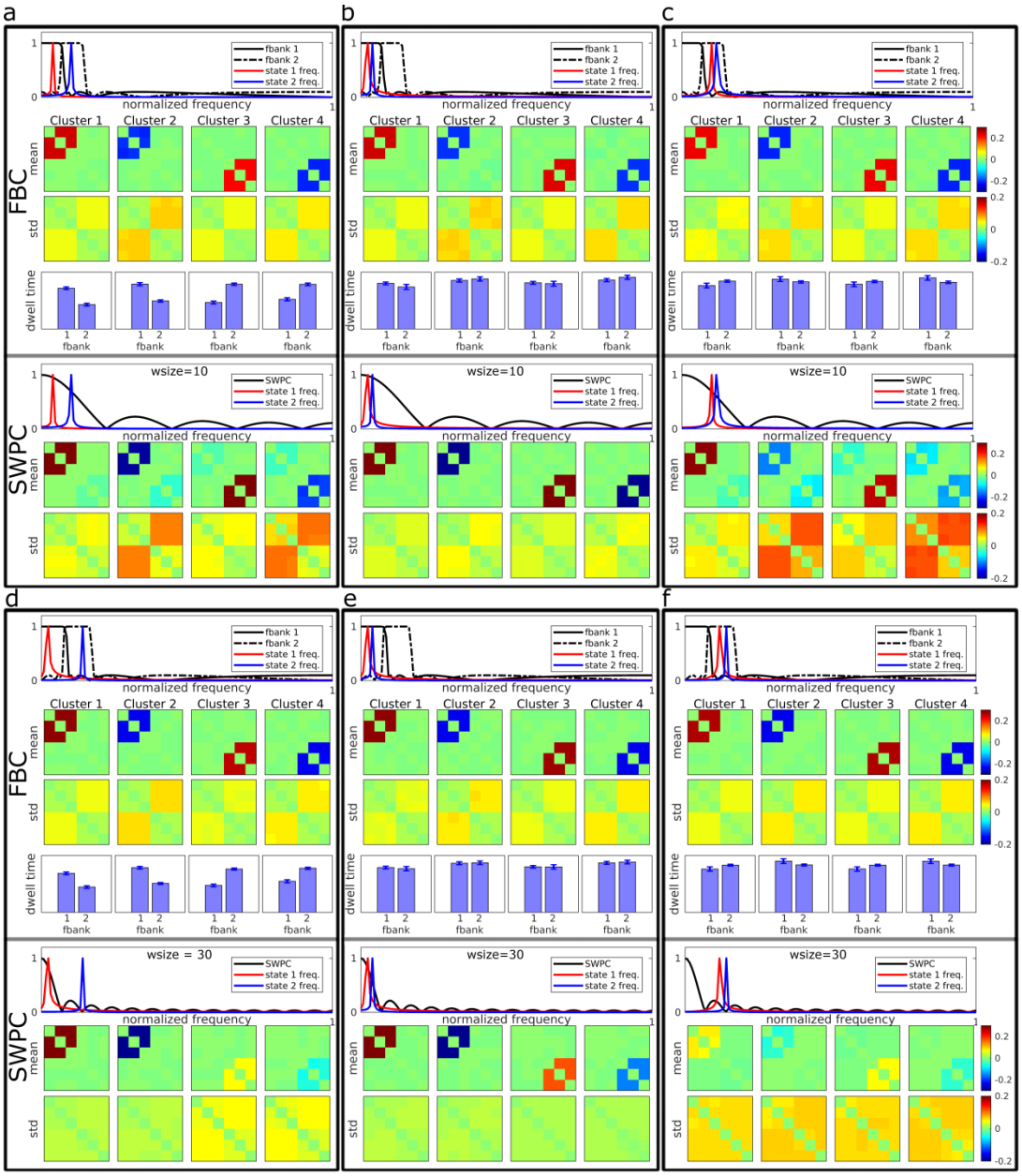

Figure 3. simulation results. Each figure (a through f) show the results from both FBC and SWPC analysis. The first four rows illustrate FBC related results while the last three rows illustrate SWPC results. The first and fifth row shows the connectivity frequency of each specific scenario in addition to the frequency response of filter banks (first row) and sliding window (the fifth row) used for the analysis. The second and sixth rows show the mean of estimated cluster centroids (i.e. connectivity states) from all simulations for FBC (second row) and SWPC (sixth row) approaches. The third and seventh rows show the std of the estimated cluster centroids for FBC (third row) and SWPC (seventh row) approaches. The fourth row shows the frequency profile of the estimated cluster centroids for FBC (this information is exclusive to the FBC approach and is one of this method strengths). Figures a through c is the scenario where the SWPC sliding window is chosen correctly (connectivity frequencies are included in the main lobe of the sliding window for all three cases). In these cases, SWPC has managed to estimate states correctly in the three cases but when at least one of the states has higher frequencies where SWPC main lobe has lower value (figure a and c), SWPC is not able to distinguish between different states well (the mean matrices show both state patterns). In contrast, FBC has managed to estimate the 2 states very distinctly (e.g. the state 2 pattern does not appear in both cluster 1 and 2 in figure c unlike SWPC results). In addition, FBC is showing superior std (i.e. lower) in these cases. Figures d through f illustrate the results from the second scenario where SWPC window size is not chosen correctly (either because of investigator mistake or Pearson correlation technical limitations). Apart from the case where both state connectivity frequency is in the passband of SWPC (figure e), SWPC is not able to estimate the two states well (i.e. low

bioRxiv preprint doi: https://doi.org/10.1101/706838; this version posted July 18, 2019. The copyright holder for this preprint (which was not certified by peer review) is the author/funder. All rights reserved. No reuse allowed without permission.

values for means). In contrast, FBC does well in all three cases (high mean values). Apart from case e, where connectivity frequencies are very low and SWPC has an advantage over FBC, in the other 2 cases, std of FBC is superior too. One final note is that in the cases where the connectivity frequencies are in two separate bands (figures a and d) the connectivity frequency profiles resulted from FBC show that clusters 1 and 2 have lower frequency while clusters 3 and 4 have higher frequencies.

Figure 4 shows the correlation between the estimated clusters and the true centroids (both positive and negative matrices shown in figure 2). Based on this figure we can see that in most cases FBC performs better (has a higher correlation) with the except of the case where the connectivity frequencies are well inside the SWPC frequency window (cases b and e). Thus, if even one of the states has a higher frequency than what is covered by the SWPC window, FBC perform better. In addition, compared to SWPC, FBC shows more robust performance (i.e. FBC performance is similar between different scenarios). Finally, FBC results seem to have less variation (spread of correlation values) compared with SWPC which has only low variation in cases b and d (essentially best case scenarios for SWPC).

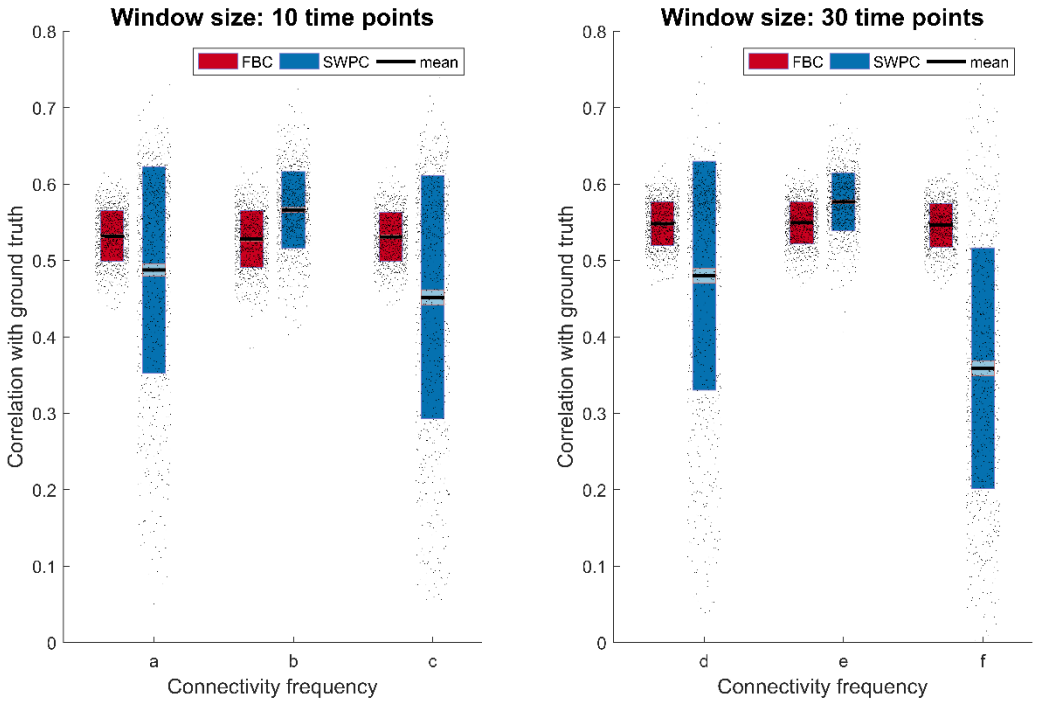

Figure 4 Correlation of estimated cluster centroids with ground truth for all simulations. The left figures show the results for the cases when the window size is 10 time points (cases a through c) while the right image is for the cases where the window size is 30 time points (cases d through f). As can be seen here FBC performs better for most of the cases, with the exception where the connectivity frequency is well in the band pass of SWPC sliding window (cases b and e; See Figure 3). In the cases where even one of the connectivity frequencies spread outside the SWPC window size (cases a, c, d and f) FBC performs better than SWPC. Note also that the FBC mean Correlation values remain mostly the same for all 6 cases. This observation combined with the fact that we are not able to know the correct window size, suggest FBC as a more robust solution.

fBIRN results

bioRxiv preprint doi: https://doi.org/10.1101/706838; this version posted July 18, 2019. The copyright holder for this preprint (which was not certified by peer review) is the author/funder. All rights reserved. No reuse allowed without permission.

As mentioned in the method section, FBC is utilized to analyze the fBIRN data set. After calculating FBC values for all component pairs, these values are clustered into 8 clusters using the k-means method. The results can be seen in Figure 5. This figure first row shows the 8 cluster centroids. The second row shows the total dwell time for each cluster centroid for all filter banks. The third row shows the same total dwell time but overall filter banks with the aim of using these values to compare HC with SZ.

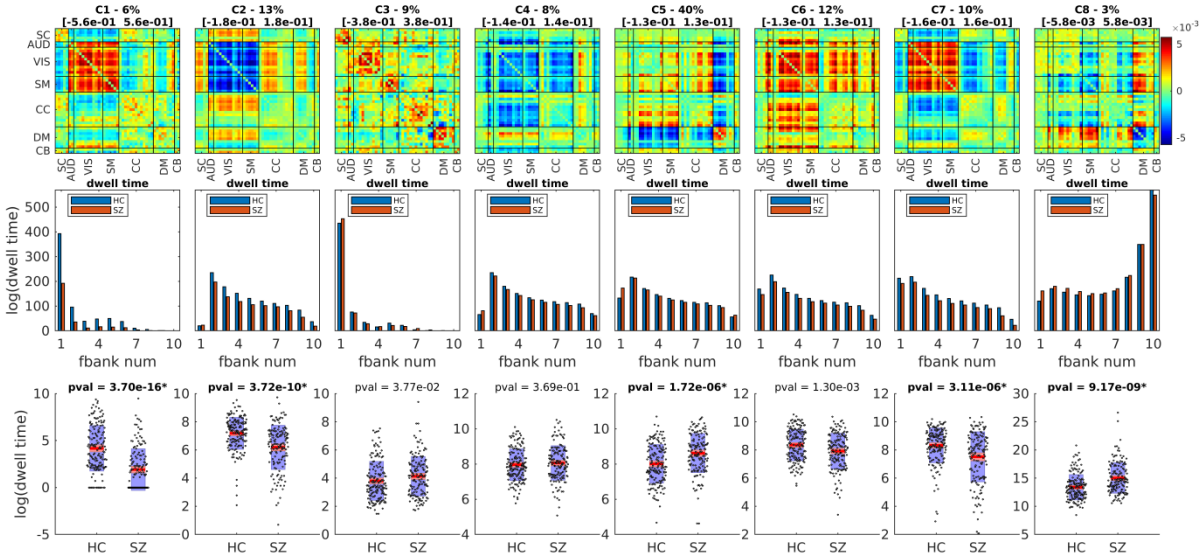

Figure 5. fBIRN FBC results. The first row shows the cluster centroids of the 8 estimated clusters where the title shows the ratio of each state occurrence and range of each state centroid (e.g. for C1 -5.6e-01 is blue where 5.6e-01 is red). The second row shows each cluster frequency profile (dwell time of each cluster for each band) for HC and SZ separately. The third row compares the dwell time across all bands between HC and SZ (the title of each figure contains the comparison p-value where the significant ones are in bold font). The first observation we can make is that FBC has resulted in 3 states (states 2, 4 and 8) which show opposite patterns to some other states (states 7,6 and 5 respectively). These opposite patterns are not visible within the SWPC results and all of them show a more high-pass frequency profile (possibly the reason these are not visible in the SWPC results). These opposite patterns might point to the presence of connectivity oscillation as designed in our simulations. Another observation we can make is that states 1 and 3 show very strong low-pass frequency profile where HC tend to spend more in state 1 while SZ spend more time in state 3. Interestingly, these two sates are very similar to the static connectivity calculated from HC and SZ separately (see Figure 6). Based on the total dwell time across all bands, we see that HCs tend to spend more time in state pairs 2 and 7 while SZ tend to stay more in states 5 and 8. States 8 is a finding exclusive to FBC and show negative connectivity between SM and SC/AUD/VIS domains. This state is quite similar to the state reported by (Yaesoubi et al., 2017) for SZ.

Based on the total dwell time per filter bank figures (Figure 5 second row), we see that we essentially have 3 types of clusters. The first clusters happen dominantly in the first filter bank (they have very low-pass nature). Cluster 1 and 3 belong to this category. The second category of clusters happen in middle frequencies (they have band-pass nature). Clusters 2, 4, 5, 6 and 7 belong to this category. Cluster 8 belong to the last category which happens dominantly in very high frequency (it has high pass-nature).

Figure 6 shows the static FNC (FNC calculated over the whole time series using Pearson correlation) of HC and SZ groups separately. Looking at Figure 6, we can see that the HC group has a stronger positive connectivity block in AUD, VIS and SM functional domains compared to SZ static FNC. Comparing these results to the 2 low-pass clusters in Figure 5 (Cluster 1 and 3), we can see a resemblance between cluster 1 and static FNC of HC (both have strong the strong connectivity block in AUD, VIS and SM domains) and cluster 3 and FNC of HC. This can also be verified using Figure 8. Based on this figure, HC static FNC highest correlation is with FBC cluster 1 while SZ static FNC has a higher correlation with FBC cluster 3. Another

bioRxiv preprint doi: https://doi.org/10.1101/706838; this version posted July 18, 2019. The copyright holder for this preprint (which was not certified by peer review) is the author/funder. All rights reserved. No reuse allowed without permission.

observation that can enhance this comparison is that HC tends to spend significantly more time in Cluster 1 compared to SZ (Figure 5 last row). SZ tend to stay more in cluster 4 compared to HC but this difference is not significant.

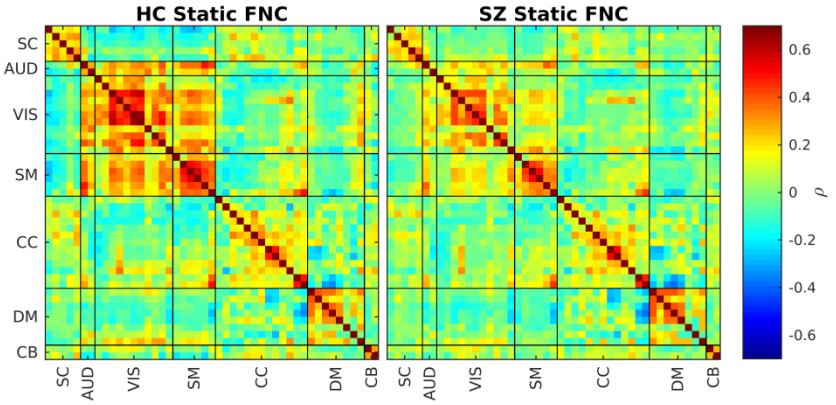

Figure 6. sFNC for HC and SZ. Patterns are similar to these in both FBC (Figure 5) and SWPC (Figure 7) result. i.e. static connectivity information is present in dFNC results. In contrast to the SWPC method, FBC enable us to study the frequency profile of the estimated states and therefore we can identify states showing a static like nature (states 1 and 3 in the current work; Figure 5)

Figure 7 shows the 8 clusters resulted from SWPC. Comparing Figure 7 with Figure 5, we can see that all the clusters resulting from SWPC are repeated in FBC results. This statement can be verified using Figure 8. As seen in the aforementioned figure, all SWPC clusters have a high correlation with at least one of the FBC clusters. In contrast, 3 of FBC clusters are not visible in SWPC results, namely, clusters 2, 4 and 7. From These 3 clusters, clusters 2 and 4 have low dwell time in the first filter bank (where SWPC window in the frequency domain has the strongest value) and cluster 8 has very high dwell time in the last filter bank (where SWPC window has very low values in frequency domains). An additional observation we can make on these 3 clusters is that they are quite opposite of 3 other FBC clusters. Namely cluster 2 is opposite of cluster 1, cluster 4 is opposite of cluster 6, cluster 8 is opposite of cluster 5. This is quite similar to our simulation results (Figure 3).

Looking at the comparison between HC and SZ dwell times of FBC results (Figure 5 last row), we can see that, from the 8 comparisons, 5 are significant after correcting for multiple comparisons. HCs tend to stay more in clusters 1, 2 and 7, while SZs tend to stay more in clusters 5 and 8. As mentioned previously, cluster 1, 2 and 7 are related while cluster 5 is related to cluster 8.

bioRxiv preprint doi: https://doi.org/10.1101/706838; this version posted July 18, 2019. The copyright holder for this preprint (which was not certified by peer review) is the author/funder. All rights reserved. No reuse allowed without permission.

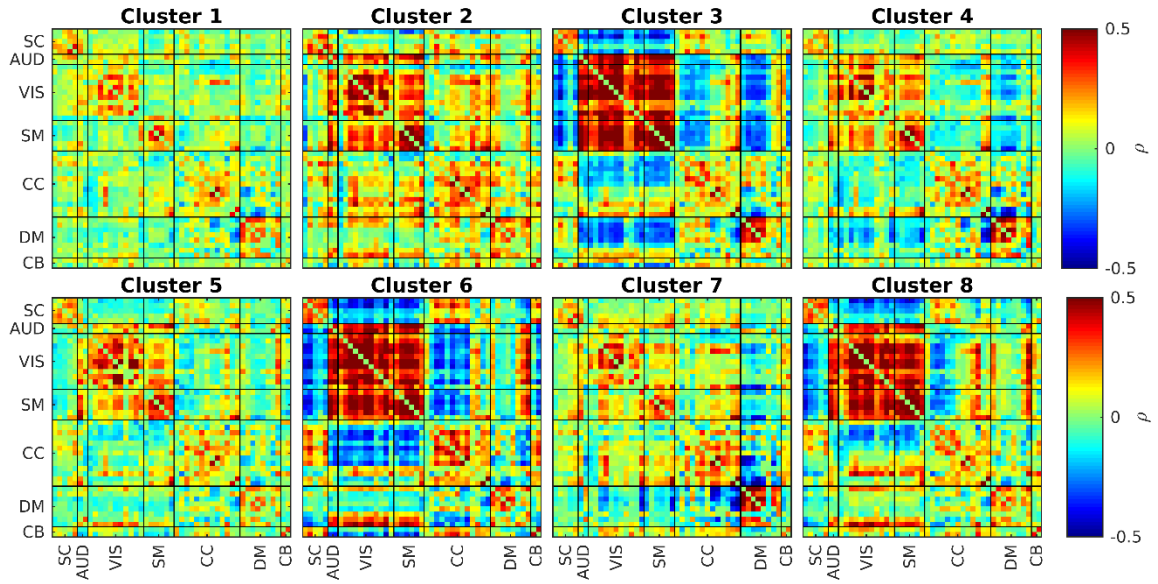

Figure 7. fBIRN SWPC results. As explained in the method section SWPC results are low-passed by nature. We can verify this claim by comparing these clusters with clusters resulted from FBC. SWPC clusters are highly similar to FBC clusters 1, 3, 5, 6 and 7 (see Figure 8). Based on Figure 5, all these FBC clusters have a very low-pass frequency profile (dwell time at the first band is quite comparable to other bands). In contrast, FBC clusters 2, 4 and 8 have different frequency profiles. For FBC states 2 and 4 dwell time of the first band is low compared to other bands while for state 8, dwell time for the highest band is very high. Therefore, using SWPC, we are only able to investigate low-pass connectivity patterns where faster changes in connectivity (possibly can give us interesting information) can go undetected.

bioRxiv preprint doi: https://doi.org/10.1101/706838; this version posted July 18, 2019. The copyright holder for this preprint (which was not certified by peer review) is the author/funder. All rights reserved. No reuse allowed without permission.

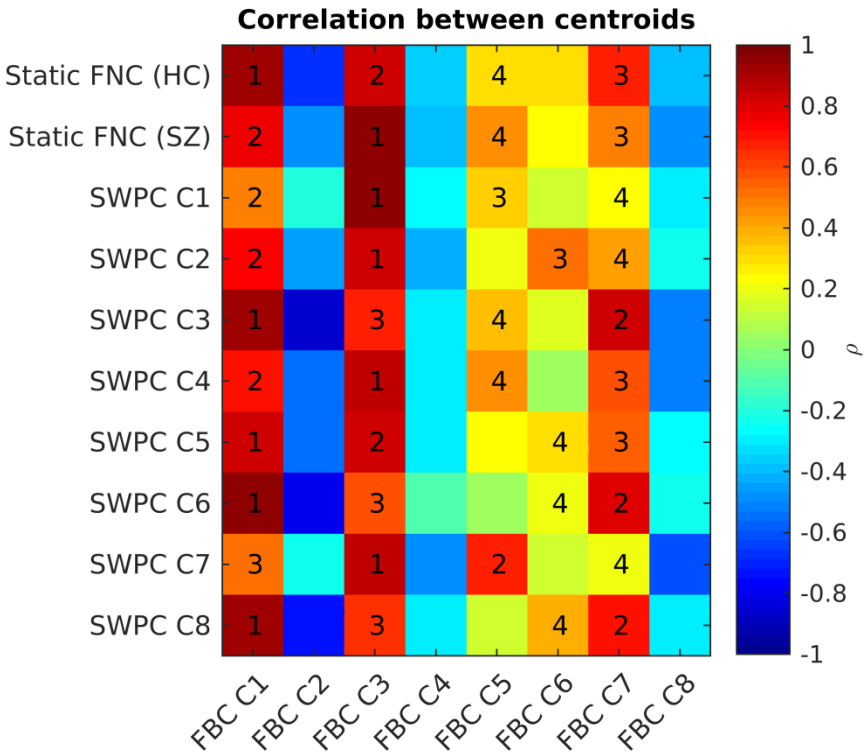

Figure 8. The similarity between sFNC and dFNC cluster centroids resulted from SWPC and those from FBC. The number in each matrix elements shows the order of FBC clusters similarity for each row (e.g. for SWPC C7 row, FBC C3 has the highest similarity with SWPC C7). We can see that sFNC calculated from HC is similar to FBC state 1 while SZ sFNC is similar to state 3. Interestingly based on the FBC results (Figure 5), these two states show very low-pass frequency profile and HC tend to stay more in state 1 ($p<0.01$) while SZ stays more in state 3 ($p=0.03$, not significant). In addition, clusters resulted from SWPC are very similar to FBC states 1, 3, 5, 6 and 7 where all of them show low-pass frequency profiles. There is no SWPC cluster similar to FBC states 2, 4 and 8. i.e. these 3 states would go undetected using SWPC where two of these states (states 2 and 8) show a significant difference for dwell time between HC and SZ, pointing to a possible loss of interesting information.

Discussion

In this work, we developed a new method (FBC) to estimate dFNC that is not limited to low frequency connectivity. We first designed simulations and showed that FBC enables us to estimate high-frequency changes in functional connectivity while typical SWPC might miss these changes (either because of the wrong chose of window size or due to methodological limitations of Pearson correlation). We then used FBC to analyze FBIRN dataset and found 8 distinct connectivity states each with their own unique frequency profile. We showed that FBC is able to estimate the states resulting from SWPC in addition to some other states that go undetected using SWPC because of their higher frequency profile. In addition, FBC enables us to explore the frequency profile of connectivity patterns in the whole frequency range.

Activation frequency vs. connectivity frequency:

As we mentioned in the introduction section, many studies have tried to explore the frequency profile of connectivity using different methods. The majority of these methods perform frequency tiling in the activity domain and then calculate connectivity. Then they proceed to make indirect inferences about the connectivity frequency profile. This is problematic as the relationship between the activity domain and

bioRxiv preprint doi: https://doi.org/10.1101/706838; this version posted July 18, 2019. The copyright holder for this preprint (which was not certified by peer review) is the author/funder. All rights reserved. No reuse allowed without permission.

connectivity domain is unclear at best and depends on the specific methods used. Many methods estimate connectivity (i.e. transform the activity domain into the connectivity domain) using highly nonlinear systems and therefore the frequency information is distorted in this transformation. For example, looking at the SWPC formula (Eq.1) we see that $\mu_x(t)$ is subtracted from $x(i)$ and the resulting value is divided by $\sigma_x(t)$. This part in itself distort the frequency profile of x. In addition to calculating the correlation $[x(i) - \mu_x(t)]/\sigma_x(t)$ is multiplied by $[y(i) - \mu_y(t)]/\sigma_y(t)$ further distorting the frequency information. Therefore, using frequency information within the activity domain to infer frequency related information specific to connectivity is not straightforward. Some studies overlook this detail when studying connectivity frequency profile. For example, Li et. al. used frequency tiling in the activity domain to conclude that "oxygen correlation is band limited" (Li et al., 2015). In another study, Yaesoubi et al, used the wavelet transform to decompose the activity time series into different time-frequency bands and then calculate coherence. Several observations about connectivity frequencies are then made (Yaesoubi et al., 2017). In our view, these kinds of statements can be misleading as the frequency profile is not directly studied in the connectivity space and therefore it does not enable us to make claims about the connectivity frequency profile. Rather they show that connectivity is caused by signals (i.e. activity) from specific frequency bands.

We believe to make claims about the connectivity frequency profile it is important to implement frequency tiling directly in the connectivity space and differentiate between the frequency profile of activity (estimated from time series themselves) and the frequency profile of the connectivity. The relationship between these two is not clear, so using knowledge about time series frequencies to make inferences regarding the connectivity frequency profile is not as straightforward as some studies suggest (Leonardi and Van De Ville, 2015).

FBC performs frequency tiling in the connectivity domain

In this work, we have proposed an approach called FBC to estimate dFNC which does not make any assumption about the frequency profile of connectivity. This is in contrast with SWPC, which applies a low-pass filter when calculating dFNC. Using k-means clustering to summarize FBC results, we found that in addition to states resulted from SWPC, we can estimate some other states exclusive to FBC (see Figure 5). In addition, because of the frequency tiling nature of our method (which was implemented in connectivity domains) we are able to discuss the frequency profile of the estimated connectivity patterns. In many dFNC studies, it is reported that one state (typically from SWPC) tends to be quite similar to the static connectivity (Damaraju et al., 2014; Faghiri et al., 2018). In this study, we see that 2 states have strong low frequency profiles (states 1 and 3; see Figure 5). State 1 is quite similar to sFNC resulted from HC individuals while the other state, state 3, is similar to sFNC resulted from SZ (see Figure 8 for correlation between different states). One possible conclusion from this observation is that FBC enables us to distinguish between states that show more static like behavior (states that show low-pass frequency profile) and others which are more dynamic (states that show high or band-pass frequency profile). This feature of FBC can be utilized so that we have a full picture of FNC in all its frequencies. i.e, study both static and dynamic FNC patterns simultaneously. One possible modification of our approach is using very narrow passband for the first filter bank (which includes pure sFNC) so that the first filter represents lower frequencies of FNC (more static like FNC).

bioRxiv preprint doi: https://doi.org/10.1101/706838; this version posted July 18, 2019. The copyright holder for this preprint (which was not certified by peer review) is the author/funder. All rights reserved. No reuse allowed without permission.

sFNC repeats in higher frequencies with lower Cognitive Control connectivity

Similar to the states reported in our earlier work (Damaraju et al., 2014), several of the states resulted from SWPC approach (Figure 7) are quite similar to each other (states that show similar patterns to overall sFNC). We can see two states similar to these in FBC results too (namely states 1 and 7). Unlike SWPC results, here we can see that while state 1 shows a very strong low-pass frequency profile, state 7 shows a more uniform frequency distribution across bands (Second row Figure 5). Again because of the frequency tiling of FBC, we have some added information in regard to the frequency profile of connectivity patterns that we can investigate. Figure 9 illustrates these two states while showing the difference between their normalized versions. As seen in the rightmost of Figure 9, cluster 7 has lower CC connectivity in general. One possible observation we can make here is that cluster 1 (which is quite similar to HC sFNC and has a very low-frequency profile) occurs in higher frequencies in the form of cluster 7 with smaller CC connectivity values. We speculate that CC (especially intraconnectivity within CC components) are lower in higher frequencies. This point needs further examination in future works.

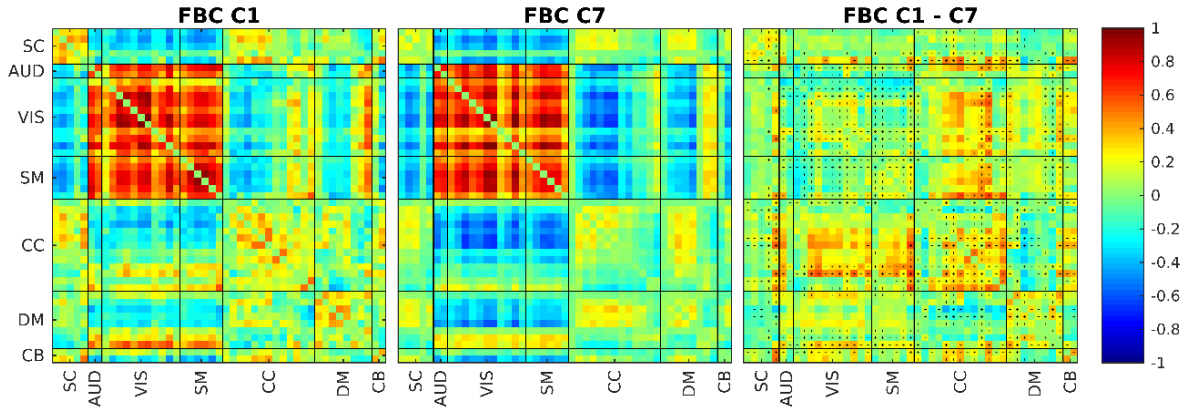

Figure 9. A close look at FBC clusters 1 and 7. The rightmost figure shows the difference between cluster 1 (left) and cluster 7 (middle). The positive sign in each entry for the difference matrix indicate the entries where C1 is positive. Based on this figure we can see that C1 is very similar to C7 but it has higher connectivity values for CC (both connectivity within CC and between CC and other networks). This can mean that sFNC connecitivity patterns are repeated in higher frequencies too but with lower connectivity in CC.

Anticorrelation between somatomotor and subcortical/visual/auditory networks

FBC has resulted in two unique states, 5 and 8, which are not visible in SWPC clusters (no SWPC cluster show the highest correlation with these states). SZ tend to significantly spend more times in these two states compared to HC ($P<0.01$). State 8 shows an interesting pattern. There is a negative correlation between SM networks and the SC, AUD and VIS networks. This pattern has also been reported in previous work (Yaesoubi et al., 2017). We have reported a high-pass frequency profile for this pattern (Figure 4), while Yaesoubi et al., reported a more band-pass profile for this pattern. We believe the reason for this difference is that our method utilize frequency profile in connectivity domain while Yaesoubi et al., utilize it in activity domain. This in turns, allow us to connect our results to connectivity frequency more directly. Several studies have reported the presence of connectivity between motor and sensory regions in healthy

bioRxiv preprint doi: https://doi.org/10.1101/706838; this version posted July 18, 2019. The copyright holder for this preprint (which was not certified by peer review) is the author/funder. All rights reserved. No reuse allowed without permission.

controls (D'Ausilio et al., 2009; Londei et al., 2010). A reduction in connectivity between these regions in SZ has been reported in the past years (Berman et al., 2016; Kaufmann et al., 2015). In our work, we do not find a reduction in the connectivity between SM and VIS/AUD network, rather we show that SZ spends more time in states showing strong anticorrelation between these networks.

Dynamic connectivity highlights oscillations between two opposite patterns

Another observation we can make based on the states estimated using FBC (Figure 5) is that there are pairs of states (undetected by SWPC) which show opposite connectivity patterns (SWPC identifies only one of these). In our case, states 2, 4 and 8 show opposite connectivity patterns of states 7, 6 and 5 respectively. One interesting insight about states 2, 4 and 8 is that they exhibit a more high-pass frequency profile compared to the other states. This is possibly the reason that these states are not estimated using SWPC. It is unlikely that these opposite patterns are due to an alteration in phase caused by the analysis since, as mentioned in the methods section, we used forward-backward filtering. Another explanation can be that these states are spurious estimations caused by the high-frequency nature of the filter banks as discussed by (Leonardi and Van De Ville, 2015). We cannot rule out this possibility completely but because these states show the opposite patterns of some other low-pass states this is unlikely. To further investigate, we removed the low frequency information of SWPC with different high-pass filters (forward-backward filtering) and then performed k-means clustering. Figure 10 shows the resulting clusters using different high pass filters. When removing the low frequency information, we obtain these opposite clusters (e.g. C3, Figure 10, quite similar to FBC cluster 2). Another possible explanation for these opposite patterns is that, similar to how the simulation was designed, the dynamic connectivity patterns oscillate between two opposite patterns. Unlike the simulation, the negative patterns (states 2, 4 and 8) show a higher frequency profile compared to their more low-pass counterparts, but this could reflect asymmetric oscillatory behavior (e.g. more rapid return from the negative patterns). This is an interesting observation; however future work should be designed to further explore the possibility that connectivity indeed oscillates between two opposite connectivity patterns. In addition, the biological/clinical meaning of this view should be explored further.

bioRxiv preprint doi: https://doi.org/10.1101/706838; this version posted July 18, 2019. The copyright holder for this preprint (which was not certified by peer review) is the author/funder. All rights reserved. No reuse allowed without permission.

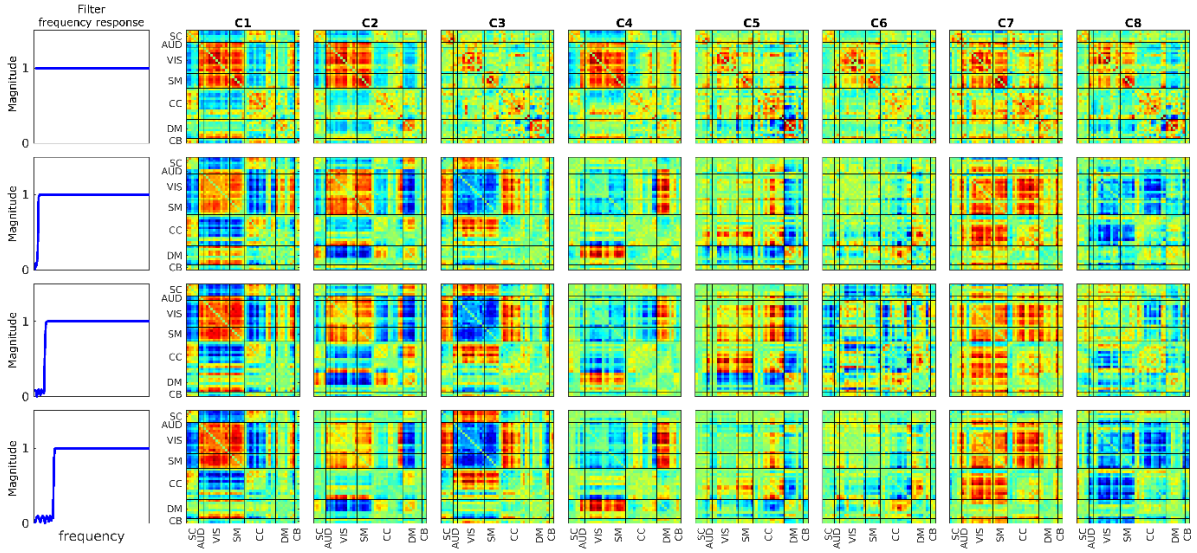

Figure 10. high-passed SWPC results. To verify FBC results we removed low frequency information of SWPC using different high-pass filters and then used k-means clustering. The first row is essentially unfiltered SWPC results while the next three rows are SWPC results using different filters. As seen in the last three row we have clusters similar to FBC clusters in SWPC results too (cluster 3, 4 and 8). The only reason these clusters were not estimated using unfiltered SWPC is because SWPC frequency response function attenuate all frequencies above zero even in its band-pass.

A systematic view of estimations

We believe that any analysis steps (including statistical estimators) can be viewed as a system and benefit from the extensive work done in system design field (Bentley et al., 2000). In this work, we examined SWPC and proposed an approximate system diagram for it (Figure 1.a). This way of thinking about SWPC facilitated our conclusion that SWPC has a low-pass filter inherent to its formula and led to our proposed more comprehensive FBC solution involving the use of a filter bank instead of a low-pass filter (Figure 1). The use of filter banks as proposed in the current work is only one possibility, for future work we can use custom h(t) modules to extract specific information. For example, one possible choice is wavelet transform in the place of subsystem 2 (wavelet can be viewed as a system itself). Another possibility is to improve SWPC by replacing its h(t) with an IIR low-pass filter with very sharp transition and flat band-pass (in contrast with SWPC with rectangular window where the frequency response of the filter is sinc like). This is in line with previous works where it has been suggested that SWPC window shape can be modulated to achieve better results (Mokhtari et al., 2019).

Limitations

The first limitation of the FBC approach is the subsystem used to transform activity space to connectivity space (Figure 1). In this system, we have used a window to calculate the mean and standard deviation. the problem arises when mean and std move faster than what the window can track. In this case, our estimations will be sub-optimal. To remedy this, we can use more instantaneous methods suggested for estimating correlation in future work (Shine et al., 2015). Another limitation of this method is the possibility of noise contamination in the higher frequencies. This is certainly a valid issue, though our goal in this work was to refrain from making any strong assumption about connectivity frequencies. The reason

bioRxiv preprint doi: https://doi.org/10.1101/706838; this version posted July 18, 2019. The copyright holder for this preprint (which was not certified by peer review) is the author/funder. All rights reserved. No reuse allowed without permission.

behind this decision was that we have no solid prior knowledge about connectivity frequency. In fact, to the best of our knowledge, this work is the first one that differentiates between activity and connectivity frequency profiles. Future investigators can utilize our proposed approach to study specific frequency bands.

Conclusion

In this work, we proposed a new approach to estimate dFNC called FBC. Our proposed approach does not make any strong assumption about connectivity frequency (unlike SWPC) and performs the frequency tiling in the connectivity domain (in contrast to previous works were frequency tiling was implemented in the activity domain). FBC aims to estimate connectivity in all frequencies and it enables us to investigate connectivity patterns frequency profiles. Using simulations, we showed that FBC is able to estimate even high-frequency connectivities in addition to providing information about the estimated connectivity frequencies. Utilizing FBC, we analyzed an fMRI dataset including HC and SZ. We found both sFNC and SWPC dFNC states using FBC in addition to some new connectivity states undetected by SWPC (possibly because of their high-pass nature). Finally, FBC points to a possible (new) view for connectivity. In this view, data oscillate between two opposite connectivity patterns. This view should be further explored in future work.

Conflicts of interest

Authors declare no conflict of interests.

Acknowledgements

Data collection was supported by the National Center for Research Resources at the National Institutes of Health (grant numbers: NIH 1 U24 RR021992, NIH 1 U24 RR025736-01, R01EB020407, P20GM103472, P30GM122734) and the National Science Foundation (1539067);

bioRxiv preprint doi: https://doi.org/10.1101/706838; this version posted July 18, 2019. The copyright holder for this preprint (which was not certified by peer review) is the author/funder. All rights reserved. No reuse allowed without permission.

References:

Allen, E.A., Damaraju, E., Plis, S.M., Erhardt, E.B., Eichele, T., Calhoun, V.D., 2014. Tracking whole-brain connectivity dynamics in the resting state. Cereb Cortex 24, 663-676.

Bentley, L.D., Dittman, K.C., Whitten, J.L., 2000. Systems analysis and design methods. Irwin/McGraw Hill.

Berman, R.A., Gotts, S.J., McAdams, H.M., Greenstein, D., Lalonde, F., Clasen, L., Watsky, R.E., Shora, L., Ordonez, A.E., Raznahan, A., Martin, A., Gogtay, N., Rapoport, J., 2016. Disrupted sensorimotor and social-cognitive networks underlie symptoms in childhood-onset schizophrenia. Brain 139, 276-291.

Boashash, B., 2015. Time-frequency signal analysis and processing: a comprehensive reference. Academic Press.

Calhoun, V.D., Adali, T., Pearlson, G.D., Pekar, J.J., 2001. Spatial and temporal independent component analysis of functional MRI data containing a pair of task-related waveforms. Hum Brain Mapp 13, 43-53.

Camchong, J., MacDonald, A.W., 3rd, Bell, C., Mueller, B.A., Lim, K.O., 2011. Altered functional and anatomical connectivity in schizophrenia. Schizophr Bull 37, 640-650.

Chang, C., Glover, G.H., 2010. Time-frequency dynamics of resting-state brain connectivity measured with fMRI. NeuroImage 50, 81-98.

D'Ausilio, A., Pulvermuller, F., Salmas, P., Bufalari, I., Begliomini, C., Fadiga, L., 2009. The motor somatotopy of speech perception. Curr Biol 19, 381-385.

Damaraju, E., Allen, E.A., Belger, A., Ford, J.M., McEwen, S., Mathalon, D.H., Mueller, B.A., Pearlson, G.D., Potkin, S.G., Preda, A., Turner, J.A., Vaidya, J.G., van Erp, T.G., Calhoun, V.D., 2014. Dynamic functional connectivity analysis reveals transient states of dysconnectivity in schizophrenia. Neuroimage Clin 5, 298-308.

Di Martino, A., Scheres, A., Margulies, D.S., Kelly, A.M., Uddin, L.Q., Shehzad, Z., Biswal, B., Walters, J.R., Castellanos, F.X., Milham, M.P., 2008. Functional connectivity of human striatum: a resting state FMRI study. Cereb Cortex 18, 2735-2747.

Erdeniz, B., Serin, E., Ibadi, Y., Tas, C., 2017. Decreased functional connectivity in schizophrenia: The relationship between social functioning, social cognition and graph theoretical network measures. Psychiatry Res Neuroimaging 270, 22-31.

Erhardt, E., Allen, E., Damaraju, E., Calhoun, V., 2011. On network derivation, classification, and visualization: a response to Habeck and Moeller. Brain Connect.

Faghiri, A., Stephen, J.M., Wang, Y.P., Wilson, T.W., Calhoun, V.D., 2018. Changing brain connectivity dynamics: From early childhood to adulthood. Hum Brain Mapp 39, 1108-1117.

Hutchison, R.M., Womelsdorf, T., Allen, E.A., Bandettini, P.A., Calhoun, V.D., Corbetta, M., Della Penna, S., Duyn, J.H., Glover, G.H., Gonzalez-Castillo, J., Handwerker, D.A., Keilholz, S., Kiviniemi, V., Leopold, D.A., de Pasquale, F., Sporns, O., Walter, M., Chang, C., 2013a. Dynamic functional connectivity: promise, issues, and interpretations. Neuroimage 80, 360-378.

Hutchison, R.M., Womelsdorf, T., Gati, J.S., Everling, S., Menon, R.S., 2013b. Resting-state networks show dynamic functional connectivity in awake humans and anesthetized macaques. Hum Brain Mapp 34, 2154-2177.

Iraji, A., Deramus, T.P., Lewis, N., Yaesoubi, M., Stephen, J.M., Erhardt, E., Belger, A., Ford, J.M., McEwen, S., Mathalon, D.H., Mueller, B.A., Pearlson, G.D., Potkin, S.G., Preda, A., Turner, J.A., Vaidya, J.G., van Erp, T.G.M., Calhoun, V.D., 2019a. The spatial chronnectome reveals a dynamic interplay between functional segregation and integration. Hum Brain Mapp 40, 3058-3077.

Iraji, A., Fu, Z., Damaraju, E., DeRamus, T.P., Lewis, N., Bustillo, J.R., Lenroot, R.K., Belger, A., Ford, J.M., McEwen, S., Mathalon, D.H., Mueller, B.A., Pearlson, G.D., Potkin, S.G., Preda, A., Turner, J.A., Vaidya,

bioRxiv preprint doi: https://doi.org/10.1101/706838; this version posted July 18, 2019. The copyright holder for this preprint (which was not certified by peer review) is the author/funder. All rights reserved. No reuse allowed without permission.

J.G., van Erp, T.G.M., Calhoun, V.D., 2019b. Spatial dynamics within and between brain functional domains: A hierarchical approach to study time-varying brain function. Hum Brain Mapp 40, 1969-1986.
Jafri, M.J., Pearlson, G.D., Stevens, M., Calhoun, V.D., 2008. A method for functional network connectivity among spatially independent resting-state components in schizophrenia. Neuroimage 39, 1666-1681.
Kaufmann, T., Skatun, K.C., Alnaes, D., Doan, N.T., Duff, E.P., Tonnesen, S., Roussos, E., Ueland, T., Aminoff, S.R., Lagerberg, T.V., Agartz, I., Melle, I.S., Smith, S.M., Andreassen, O.A., Westlye, L.T., 2015. Disintegration of Sensorimotor Brain Networks in Schizophrenia. Schizophr Bull 41, 1326-1335.
Kucyi, A., Davis, K.D., 2014. Dynamic functional connectivity of the default mode network tracks daydreaming. Neuroimage 100, 471-480.
Leonardi, N., Van De Ville, D., 2015. On spurious and real fluctuations of dynamic functional connectivity during rest. NeuroImage 104, 430-436.
Li, J.M., Bentley, W.J., Snyder, L.H., 2015. Functional connectivity arises from a slow rhythmic mechanism. Proc Natl Acad Sci U S A 112, E2527-2535.
Liu, X., Duyn, J.H., 2013. Time-varying functional network information extracted from brief instances of spontaneous brain activity. Proc Natl Acad Sci U S A 110, 4392-4397.
Londei, A., D'Ausilio, A., Basso, D., Sestieri, C., Gratta, C.D., Romani, G.L., Belardinelli, M.O., 2010. Sensory-motor brain network connectivity for speech comprehension. Hum Brain Mapp 31, 567-580.
Mallat, S., 1999. A wavelet tour of signal processing. Elsevier.
Mennigen, E., Rashid, B., Calhoun, V.D., 2019. Connectivity and dysconnectivity: A brief history of functional connectivity research in schizophrenia and future directions. In: Munsell, B.C., Wu, G., Bonilha, L., Laurienti, P.J. (Eds.), Connectomics. Academic Press, pp. 123-154.
Mitra, S.K., Kuo, Y., 2006. Digital signal processing: a computer-based approach. McGraw-Hill New York.
Mokhtari, F., Akhlaghi, M.I., Simpson, S.L., Wu, G., Laurienti, P.J., 2019. Sliding window correlation analysis: Modulating window shape for dynamic brain connectivity in resting state. Neuroimage 189, 655-666.
Oppenheim, A.V., 1999. Discrete-time signal processing. Pearson Education India.
Ou, J., Xie, L., Wang, P., Li, X., Zhu, D., Jiang, R., Wang, Y., Chen, Y., Zhang, J., Liu, T., 2013. Modeling brain functional dynamics via hidden Markov models. 2013 6th International IEEE/EMBS Conference on Neural Engineering (NER), pp. 569-572.
Potkin, S.G., Ford, J.M., 2009. Widespread Cortical Dysfunction in Schizophrenia: The FBIRN Imaging Consortium. Schizophr Bull 35, 15-18.
Rabiner, L.R., Kaiser, J.F., Herrmann, O., Dolan, M.T., 1974. Some Comparisons between Fir and Iir Digital-Filters. Bell System Technical Journal 53, 305-333.
Sakoglu, U., Pearlson, G.D., Kiehl, K.A., Wang, Y.M., Michael, A.M., Calhoun, V.D., 2010. A method for evaluating dynamic functional network connectivity and task-modulation: application to schizophrenia. MAGMA 23, 351-366.
Shine, J.M., Koyejo, O., Bell, P.T., Gorgolewski, K.J., Gilat, M., Poldrack, R.A., 2015. Estimation of dynamic functional connectivity using Multiplication of Temporal Derivatives. NeuroImage 122, 399-407.
Skudlarski, P., Jagannathan, K., Anderson, K., Stevens, M.C., Calhoun, V.D., Skudlarska, B.A., Pearlson, G., 2010. Brain connectivity is not only lower but different in schizophrenia: a combined anatomical and functional approach. Biol Psychiatry 68, 61-69.
Thompson, W.H., Fransson, P., 2015. The frequency dimension of fMRI dynamic connectivity: Network connectivity, functional hubs and integration in the resting brain. Neuroimage 121, 227-242.
van den Heuvel, M.P., Hulshoff Pol, H.E., 2010. Exploring the brain network: a review on resting-state fMRI functional connectivity. Eur Neuropsychopharmacol 20, 519-534.

bioRxiv preprint doi: https://doi.org/10.1101/706838; this version posted July 18, 2019. The copyright holder for this preprint (which was not certified by peer review) is the author/funder. All rights reserved. No reuse allowed without permission.

Yaesoubi, M., Adali, T., Calhoun, V.D., 2018. A window-less approach for capturing time-varying connectivity in fMRI data reveals the presence of states with variable rates of change. Hum Brain Mapp 39, 1626-1636.

Yaesoubi, M., Allen, E.A., Miller, R.L., Calhoun, V.D., 2015. Dynamic coherence analysis of resting fMRI data to jointly capture state-based phase, frequency, and time-domain information. NeuroImage 120, 133-142.

Yaesoubi, M., Miller, R.L., Bustillo, J., Lim, K.O., Vaidya, J., Calhoun, V.D., 2017. A joint time-frequency analysis of resting-state functional connectivity reveals novel patterns of connectivity shared between or unique to schizophrenia patients and healthy controls. Neuroimage Clin 15, 761-768.